A 3-D DNS and experimental study of the effect of the recirculating flow pattern inside a reactive kernel produced by nanosecond plasma discharges in a methane-air mixture

Maria Castela, Sergey Stepanyan, Benoit Fiorina, Axel Coussement, Olivier Gicquel, Nasser Darabiha, Christophe O. Laux

A 3-D DNS and experimental study of the effect of the recirculating flow pattern inside a reactive kernel produced by nanosecond plasma discharges in a methane-air mixture

Maria Castela [a] , Sergey Stepanyan [a], Benoit Fiorina [a], Axel Coussement [a,b], Olivier Gicquel [a], Nasser Darabiha [a], Christophe O. Laux [a]

[a] *Laboratoire EM2C, CNRS, CentraleSupélec, Université Paris-Saclay, Grande Voie des Vignes, Châtenay-Malabry cedex 92295, France*

[b] *Université Libre de Bruxelles, Ecole Polytechnique de Bruxelles, Aero-Thermo-Mechanics Laboratory, Bruxelles, Belgium*

Abstract

This paper presents 3-D DNS and experimental schlieren results used to study a non-equilibrium plasma discharge in a lean methane-air mixture. A detailed combustion mechanism and a plasma model, developed in our previous work, are used in the 3-D computations in order to study the impact of gas flow recirculation on the temporal evolution of species and gas temperature in the vicinity of the discharge zone. The results show that the formation of a fresh gas counterflow, with stagnation plane at the centre of the discharge and parallel to the electrodes, changes the topology of the hot kernel from an initial cylindrical shape to a toroidal one. This phenomenon leads to an increase of the area/volume ratio of the reactive kernel, that may result under certain conditions in kernel extinction. The results also show the importance of considering this 3-D gas flow recirculation to correctly predict the temporal evolution of the hot kernel. In particular, we show that the temperature and species concentrations in the central region of the discharge return to fresh gas conditions shortly after the end of the pulse. In the experimental case investigated here, this time is of the order of 150 μs. This result is particularly important for ignition by Nanosecond Repetitively Pulsed (NRP) discharges, because the gas conditions at the beginning of each successive pulse depend strongly on the time interval between pulses, thus on the pulse frequency

1. Introduction

The application of non-equilibrium plasmas to lean premixed or partially premixed combustion regimes can decrease ignition delay and extend flame stability domains, as demonstrated in several experimental works [1–8]. In particular, non-equilibrium plasmas produced by Nanosecond Repetitively Pulsed (NRP) discharges are an energy-efficient way to generate O radicals that readily react with the surrounding fuel molecules and enhance the combustion phenomena [9,10]. 2-D simulations of ignition of a hydrogen-air mixture by single nanosecond pulse have been performed in Tholin et al. [11]. Bak et al. [12] numerically studied the flame stabilization by multiple nanosecond discharges. Nevertheless, the gas dynamics and the thermochemical coupling between non-equilibrium plasma discharges and the reactive flow are still poorly understood. For conventional spark discharges, the effects of gas dynamics on ignition kernel propagation have already been widely studied. Thiele et al. [13,14] numerically studied the entrainment of fresh gases in the discharge channel following a spark discharge. It was shown that the blast wave generated by these spark discharges induces flow recirculation in the vicinity of the discharge channel and impacts the ignition kernel topology. However, few details on the spatial and temporal evolution of the species are given in these studies.

The problem becomes more complex for ignition by NRP discharges when ignition occurs after several pulses. This is because the conditions seen by the pulses are affected by the flow recirculation induced by previous pulses. Thus, it is important to study the evolution of species concentration and temperature field under the action of nanosecond pulsed discharges.

The aim of the present work is to study the impact of flow recirculation induced by nanosecond discharges on the ignition kernel. To this end, we have performed 3-D DNS computations with detailed combustion chemistry and a plasma model developed in our previous work [15] and we compare the simulation results with experiments. Computational and experimental schlieren images are compared for discharges in air and a methane-air mixture. We then analyze the evolution of the species and temperature fields after a discharge pulse and the impact of gas recirculation on the ignition/extinction of the kernel.

2. Methods

2.1. Experimental set-up

Nanosecond discharges in pin-to-pin geometry were initiated in air and in a premixed lean ($\phi = 0.7$) methane-air mixture at pressure p = 1 atm and temperature T = 300 K. The gap between the pins was 1 mm for all the presented experimental results. The voltage pulses applied to the electrodes were produced by a FID Technology FPG 30-100MS pulse generator. The pulses had 20 ns duration and a few tens of kV in amplitude. The electrode system was mounted inside a constant volume chamber (V = 100 cm^3) in order to perform the experiments in combustible mixture. Two sapphire optical windows of 5 cm diameter each were installed into the chamber walls to provide access for optical diagnostics. For each discharge, the voltage and the current were measured with a LeCroy high-voltage probe and a Pearson coil (model 6585), respectively. Both signals were recorded with a 1 GHz Lecroy WavePro 7100A oscilloscope. Typical voltage and current temporal evolutions for the presented experimental results in air are shown in Fig. 1. The discharge energy, calculated from the profiles, is approximately 1.4–1.5 mJ for both the air and the methane-air mixture. The schlieren technique was used to monitor the temporal evolution of the gas density distribution after the nanosecond discharge. Phase-locked schlieren images were obtained using a high-power diode laser light source CAVILUX HF and a Pi-Max4 CCD camera, with 512 × 512 pixel resolution. The schlieren system used in the present work is described in detail in Xu et al. [1].

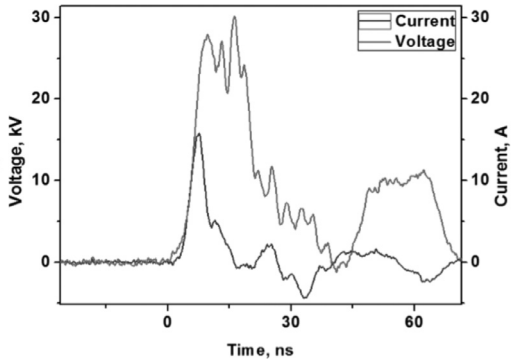

Fig. 1. Measured voltage and current waveforms during and after a single discharge in air.

2.2. Numerical set-up

Figure 2 shows a schematic representation of the computational domain. A 3-D cube with length of each side $L = 3.23$ mm was discretized with 256 non-uniformly distributed grid points. The grid spacing distribution is shown in Fig. 2b. The mesh size is around 10 μm inside the discharge channel. The overall domain contains 16.8 million grid points. Nonreflecting boundaries were imposed in all directions so that the kernel evolution occurs at constant pressure. Electrode surfaces are not taken into account in the computational domain.

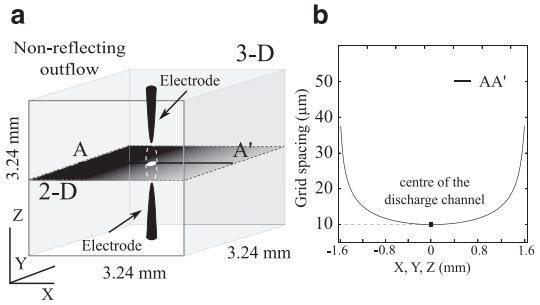

Fig. 2. Schematic representation of the 3-D computational domain used in the present work: (a) solution domain and boundary conditions. (b) mesh size distribution over the line AA'.

For both the air and the methane-air cases, the initial gas pressure and temperature are 1 atm and 300 K, respectively. For the reactive case, a quiescent mixture of methane-air with an equivalence ratio of 0.7 is uniformly distributed over the computational domain, at the beginning of the computations. The detailed combustion mechanism of Lindstedt [16] with 29 species and 141 elementary reactions is used.

2.3. *Plasma-assisted combustion model*

The numerical model of the present work is described in detail in Castela et al. [15]. Only a brief discussion of the model concepts is given here. During each high voltage nanosecond pulse, there is an increase of the kinetic energy of the electrons. The kinetic energy of the electrons is then transferred to the surrounding heavy particles through collisional processes. The rate at which these collisional processes occur depends on the reduced electric field E/N defined as the ratio of the electric field magnitude E, to the gas density N. Several detailed plasma kinetic mechanisms have been proposed in the literature [17–24] to model non-equilibrium plasma effects on combustion processes. The methods include solving the governing equations for the electric field and the electron energy, the continuity equations for neutral and excited species, and the energy, mass and momentum balance equations for the gas mixture. At the end of the discharge, the thermal non-equilibrium state can be fully characterized using this modeling strategy. However, this strategy requires prohibitive computational resources for 3-D DNS computations. The model presented in Castela et al. [15] significantly reduces these computational costs and enables multi-dimensional DNS studies of plasma-assisted ignition. Instead of solving a continuity equation for each of the additional excited states of molecules, the model captures non-equilibrium plasma effects by additional source terms in the energy and species continuity equations. The model is based on the observation that, for discharges characterised by E/N in the range of 100–400 Td (1 Td = 10^{-17}Vcm^2), about 90% of the pulse energy is stored in the electronic and vibrational states of N_2 molecules. The mechanism of excitation and relaxation of electronic states N_2(A,B,C,a',...) is given by the following two-step reaction process:

$$N_2(X) + e^- \rightarrow N_2(A, B, C, a', \ldots) + e^- \tag{1}$$

$$N_2(A, B, C, a', \ldots) + O_2 \rightarrow 2O + N_2(X) + heat \tag{2}$$

N_2(A,B,C,a',...) relaxation occurs mostly by dissociative quenching with O_2 molecules (reaction 2), on time scales of a few tens of nanoseconds, at atmospheric pressure. Therefore, this two-step process results in an ultrafast heating of the gas and ultrafast dissociation of O_2. The relaxation of vibrational states of N_2 occurs on a much longer times scales and results in slow gas heating [25].

According to this foregoing analysis, about 90% of the discharge energy translates into ultrafast heating and dissociation of O_2 molecules, and into slow gas heating. Thus, the model considers that the discharge power is divided into 3 contributions:

$$\dot{E}^p = \dot{E}^p_{chem} + \dot{E}^p_{heat} + \dot{E}^p_{vib} \tag{3}$$

The chemical $\dot{E}^p_{chem}$ and thermal $\dot{E}^p_{heat}$ terms refer to the ultrafast dissociation of O_2 molecules and gas heating, respectively. The vibrational $\dot{E}^p_{vib}$ contribution refers to the energy transferred into the vibrational states of N_2. Accordingly, the proposed set of equations to model NRP discharges in reactive mixtures is as follows:

$$\frac{\partial \rho}{\partial t} + \frac{\partial (\rho u_i)}{\partial x_i} = 0 \tag{4}$$

$$\frac{\partial (\rho u_j)}{\partial t} + \frac{\partial (\rho u_i u_j)}{\partial x_i} = -\frac{\partial p}{\partial x_j} + \frac{\partial \tau_{ij}}{\partial x_i} \tag{5}$$

$$\frac{\partial (\rho e)}{\partial t} + \frac{\partial (\rho u_i e)}{\partial x_i} = -\frac{\partial q_i}{\partial x_i} + \frac{\partial (\sigma_{ij} u_i)}{\partial x_i} + \dot{E}^p_{chem} + \dot{E}^p_{heat} + \dot{R}^p_{VT} \tag{6}$$

$$\frac{\partial (\rho e_{vib})}{\partial t} + \frac{\partial (\rho u_i e_{vib})}{\partial x_i} = \frac{\partial}{\partial x_i}\left(\rho \mathcal{D} \frac{\partial e_{vib}}{\partial x_i}\right) + \dot{E}^p_{vib} - \dot{R}^p_{VT} \tag{7}$$

$$\frac{\partial(\rho Y_k)}{\partial t} + \frac{\partial(\rho u_i Y_k)}{\partial x_i} = -\frac{\partial(\rho V_{k,i} Y_k)}{\partial x_i} + W_k \dot{\omega}_k^c + W_k \dot{\omega}_k^p \tag{8}$$

With

$$\dot{E}_{chem}^p = \eta \frac{Y_{O2}}{Y_{O2}^f}\left(1 - \frac{W_O}{W_{O2}}\frac{e_{O_2}}{e_O}\right)\dot{E}^p \tag{9}$$

$$\dot{E}_{heat}^p = \left[\alpha - \eta \frac{Y_{O2}}{Y_{O2}^f}\left(1 - \frac{W_O}{W_{O2}}\frac{e_{O_2}}{e_O}\right)\right]\dot{E}^p \tag{10}$$

$$\dot{E}_{vib} = (1-\alpha)\,\dot{E}^p \tag{11}$$

$$\dot{\mathrm{R}}_{VT}^{\,p} = \rho \frac{e_{vib} - e_{vib}^{eq}(T)}{\tau_{VT}} \tag{12}$$

The energy equation, Eq. (6), incorporates the additional source terms from the plasma discharge. Equation (7) is the additional conservation equation for the vibrational energy e_{vib}, carried by N_2 molecules, and $\mathcal{D}$ is the diffusion coefficient of N_2. The term $\dot{R}_{VT}^p$ in both Eqs. (6) and (7) refers to the relaxation rate of vibrational energy into gas heating. In Eq. (12) the equilibrium value of the vibrational energy at a given gas temperature T is given by $e_{vib}^{eq}(T) = (r\,\Theta_1)/(exp(\Theta_1/T) - 1)$, where $\Theta_1 =$ 3396 K and $r = R/W_{N_2}$, with R the gas constant and W_{N_2} the nitrogen molar mass. τ_{VT} is computed as a function of τ_{VT}^k given by the experimental correlation of [25]:

$$\tau_{VT} = \left(\frac{1}{\tau_{VT}^O} + \frac{1}{\tau_{VT}^{O_2}} + \frac{1}{\tau_{VT}^{N_2}}\right)^{-1} \tag{13}$$

$$\tau_{VT}^k = c/p_k\, exp[a_k\,(T^{-1/3} - b_k) - 18.42] \tag{14}$$

where τ_{VT}^k is the vibrational-translational relaxation time of N_2 molecules by the k^{th} collisional species partner (O_2, O and N_2). $c = 1$ atm · s, p_k is the partial pressure of the k^{th} species and a_k and b_k are experimental constants depending on the k^{th} species. In Eq. (8), $\dot{\omega}_k^p$ is the molar production rate to model the ultrafast species dissociation/formation by the plasma discharge. In the present work only O_2 and O are considered:

$$\dot{\omega}_{O_2}^p = -\frac{W_O}{W_{O2}}\,\dot{\omega}_O^p \tag{15}$$

$$\dot{\omega}_O^p = \eta\,\frac{Y_{O_2}}{Y_{O_2}^f}\,\frac{\dot{E}^p}{e_O} \tag{16}$$

$$\dot{\omega}_k^p = 0 \;\text{ if k} \neq \mathrm{O_2}\,,\,\mathrm{O} \tag{17}$$

As in Castela et al. [15], the parameter α represents the sum of the energy fractions transferred into ultrafast gas heating and dissociation of O_2, and is taken equal to 55% [26]. The parameter η represents the fraction of the pulse energy going into the dissociation of O_2 molecules, and is taken equal to 35%, according to [26]. Therefore, the fraction of the pulse energy transferred into ultrafast gas heating is given by Eq. 10 it is equal to α - η = 20% when the discharge is applied in fresh gas and O_2 is not dissociated. Even though in the experiment the electric energy is deposited within 20 ns, the collisional processes leading to O_2 dissociation and ultrafast increase of the gas temperature occur during the relaxation of the electronic excited N_2 molecules. As the model does not consider the intermediate time steps of these processes, the energy deposition characteristic time is modeled as the O_2 dissociation and temperature increase characteristic time, which according to [26] and [27] is about 50 ns. The discharge energy per unit volume, referred hereinafter as σ_{pulse}, is therefore assumed uniformly deposited within the characteristic time, $\tau_{pulse} = 50$ ns and $\dot{E}^p$ is modeled as follows:

$$\dot{E}^p(t_{per}, x_i) = \begin{cases} \frac{\sigma_{pulse}}{\tau_{pulse}} \cdot \mathcal{F}(r) & \text{if } t_{per} \leq \tau_{pulse} \\ 0 & \text{if } t_{per} > \tau_{pulse} \end{cases} \tag{18}$$

The spatial function $\mathcal{F}(r)$ defines the region where the plasma discharge occurs and is given by: $\mathcal{F}(r) = erfc\left(\frac{r}{a}\right)^b$, where $a = 690\times10^{-10}$ m, $b = 5/2$ and r is the radial (2-D computations) and longitudinal distance (3-D computations) to the centre of the discharge channel. The values of these geometric constants are fitted to model the experimental discharge radius $r = 225$ µm.

2.4. DNS solver

The model is implemented in a structured Direct Numerical Simulation solver - YWC - dedicated to compressible reactive flow simulations with detailed chemistry and multicomponent mixture averaged transport properties [28]. The spatial derivatives are computed with a 4th order centered finite-difference scheme. An 8th order filtering scheme is used for stability purpose. The code is explicit in time using a 4th order Runge-Kutta method. To capture stiff pressure waves induced by each plasma discharge, the hyper-viscosity technique developed in [29–31] is employed.

2.5. Validation of the discharge energy deposition in the numerical simulations

As discussed in Xu et al., [32], the evolution of the pressure wave and hot kernel radius early after the discharge pulse is a function of the gas temperature inside the discharge channel and the energy transferred into ultrafast gas heating. As will be discussed in the results, the gas recirculation intensity increases with the fraction of the pulse energy transferred into ultrafast gas heating. For simplicity, we keep the same values α and η as in the model

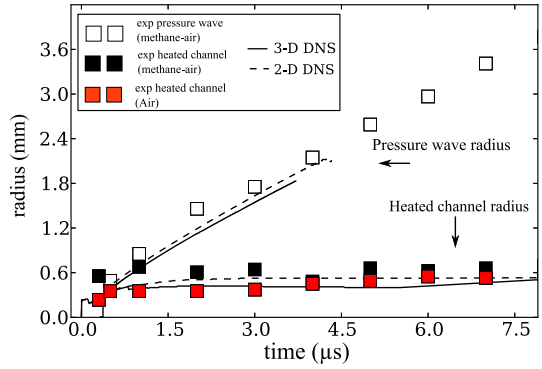

Fig. 3. Temporal evolution of the pressure wave and hot kernel radius at early instants after the discharge pulse. Symbols: experiments; Lines: computations (methane-air).

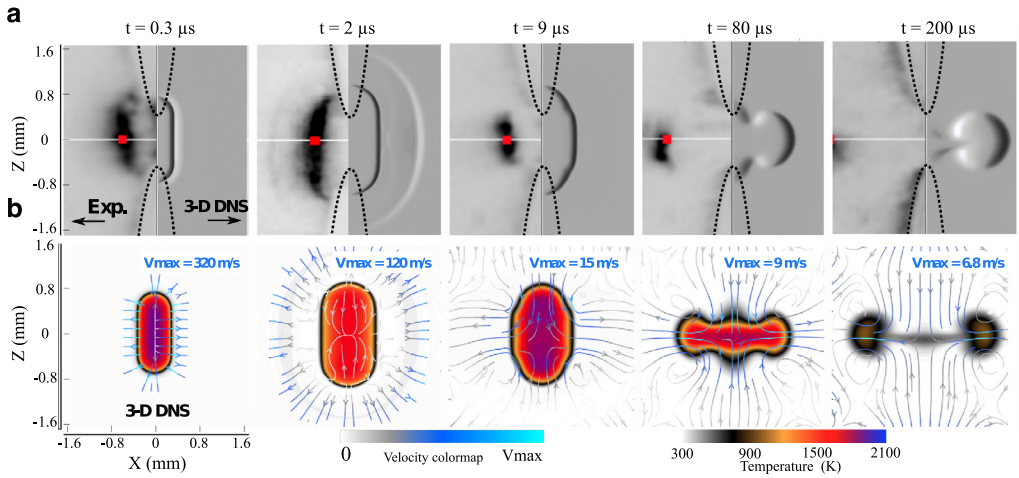

Fig. 4. Hot kernel topology captured at 5 instants after the plasma discharge in methane-air mixture: (a) Experimental (left side) and computational (right side) schlieren images. (b) Superposition of the computed gas temperature field and flow streamlines coloured by velocity magnitude. The same color map of velocity magnitude is used in for all images shown here, but the maximum value V_{max} varies and is indicated above each image.

of [15] and we adjust the total deposited energy in order to correctly predict the experimental pressure and hot kernel evolution at the first instants. Figure 3 shows the temporal evolution of the pressure wave and hot kernel radius at early instants after the discharge in air and methane-air mixture. A good agreement between the experimental and numerical hot kernel radius is obtained for an energy deposition of 0.8 mJ, which agrees reasonably well with the measured deposited energy of 1.4–1.5 mJ.

3. Results and discussion

3.1. Gas dynamics induced by a single pulse discharge

Figure 4 a shows side-by-side experimental (left) and computational (right) schlieren images captured at 5 instants following the discharge pulse in the methane-air mixture. In both experimental and numerical images, the black and grey zones are representative of maximum and null gradients of the gas density in the $x-axis$ direction, respectively. We define the extent of the hot kernel generated by the plasma discharge as the distance from the maximum of the gas density gradient (identified by the red square in Fig. 4a) to the center of the discharge channel ($x = 0$).

The ultrafast energy deposition leads to an ultrafast increase of the gas temperature and pressure inside the discharge zone. Figure 4a shows that, up to $t \approx 0.3$ µs, the hot kernel radius remains approximately equal to the discharge radius. After the ultrafast increase of the gas pressure, the gas expands. At $t \approx 0.3$ µs, a blast wave detaches from the central hot core and propagates outwards through the surrounding mixture. At $t = 2$ µs, computational and

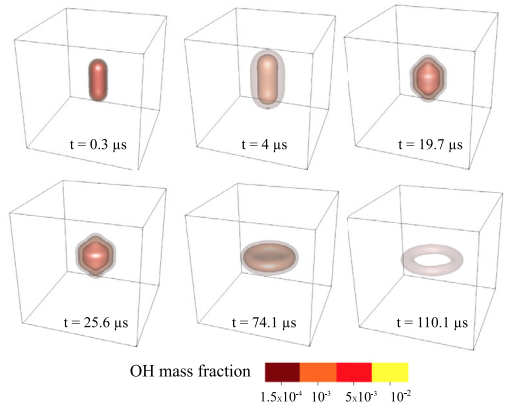

Fig. 5. Temporal and spatial evolution of the OH mass fraction after a single nanosecond plasma discharge.

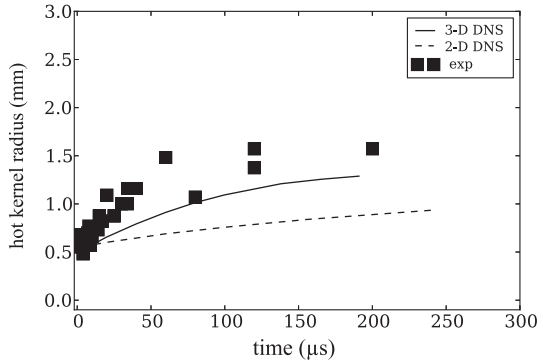

Fig. 6. Influence of gas recirculation on the evolution of the hot kernel radius . – With gas recirculation (3-D DNS), - - Without gas recirculation (2-D DNS).

experimental results show the perturbation of the gas density associated with this blast wave, as well as the increase of the hot kernel radius due to the gas expansion. The numerical simulations match the temporal evolution of the experimental hot kernel extent until well after the end of the discharge pulse.

Figure 4b shows the simulation results of the flow streamlines superposed with the gas temperature fields at the same instants as in Fig. 4a. The pulse energy is deposited inside a cylindrical channel, and therefore, as shown at $t = 2$ µs, the fluid motion induced by the blast wave in the $x - axis$ direction is stronger than along the $z - axis$. As observed at 9, 80 and 200 µs, this initial flow asymmetry creates two recirculation zones that lead to fresh gas entrainment into the discharge channel. The gas temperature at the centre of the discharge decreases from 2000 to 600 K between $t = 9$ µs and $t = 200$ µs, and the initially cylindrical hot kernel (at $t = 2$ µs) evolves into a toroidal shape. The flow pattern resembles a counterflow with a stagnation plane $z = 0$. Figure shows a 3-D visualization of the spatial and temporal evolution of the OH mass fraction. It clearly shows the evolution of the initially cylindrical shaped into a toroidal shaped kernel.

To evaluate these 3-D effects on the hot kernel growth, we performed a 2-D simulation in the plane $z = 0$ (see Fig. 2). In this 2-D simulation, the flow is symmetric and therefore, there is no gas entrainment. The kernel growth is only controlled by gas expansion. Figure 6 shows the temporal evolution of the hot kernel extent with (3-D DNS) and without (2-D DNS) gas recirculation. The results show that the extent of the hot kernel is significantly underestimated when gas recirculation is not considered. In contrast, the evolution of the hot kernel extent is much better captured by the 3-D computations. Compared to the results presented in the literature, for instance in Thiele et al. [13,14] where the geometry of the electrodes is considered, the results of the 3-D DNS presented in Fig. 6 show that the primary trend of the flow pattern is well captured by only considering the geometry of the channel where the energy is deposited.

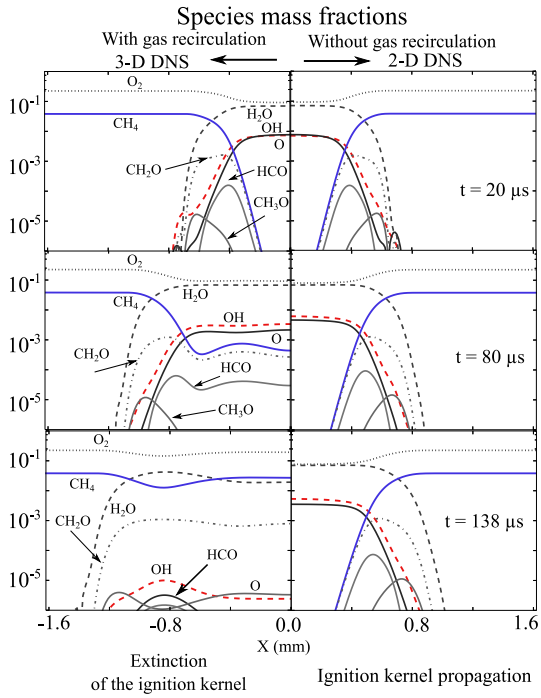

Fig. 7. Species mass fractions profiles along the line AA' depicted in Fig. 2. Species radial profiles plotted on the left side refer to the case with gas recirculation (3-D DNS), whereas the profiles plotted on the right side refer to the case without gas recirculation (2-D DNS).

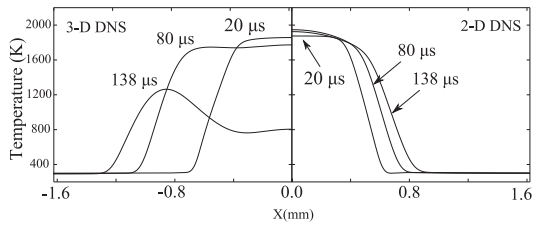

Fig. 8. Temperature radial profiles along the line AA' depicted in Fig. 2. The profiles on the left side refer to the case with gas recirculation (3-D DNS), whereas the profiles plotted on the right side refer to the case without gas recirculation (2-D DNS).

3.2. Impact of gas recirculation on species and temperature profiles in the vicinity of the discharge zone

Figure 7 shows the radial profiles in the plane $z = 0$, of major species mass fractions, at 3 different instants. Figure 8 shows the temperature radial profiles in the same plane $z = 0$ at the same instants plotted in Fig. 7. The radial profiles plotted on the left side of Figs. 7 and 8 refer to the case with gas recirculation (3-D DNS), whereas the profiles on the right side refer to the case without gas recirculation (2-D DNS). The results show, at $t = 20$ µs, the ignition of the mixture at the centre of the discharge. It also shows that the species radial profiles are similar in the 2-D and 3-D cases, which means that gas recirculation has a minimal impact up to at least $t = 20$ µs. At 80 µs, however, the species and temperature radial profiles differ significantly: for the case with recirculation, the mass fractions of CH_4, HCO and CH_2O increase at the centre of the discharge channel, and those of O and OH decrease. This is due to the recirculation flow, which cools down the channel. The mass fractions of O and OH decreases because these species recombine rapidly. CH_2O and HCO, which were initially present only at the edges of the reaction zone, are entrained into the central part of the channel and, therefore, their mass fractions increase at the centre of the discharge. The results also show that the thin reaction

zone, present at $t = 20$ μs around $x \approx -0.4$ mm, does not continue to propagate through the surrounding fresh mixture afterwards, in contrast to the 2-D case, in which the reaction zone successfully evolves into a flame front. The 3-D DNS is in agreement with the experimental results in which the ignition event was not successful after a single pulse. In fact, the extinction of the ignition kernel in the 3-D case is due to the low gas temperature upstream of the reaction zone as shown in Fig. 8 and to an increase of the diffusion heat losses, since the toroidal shape of the 3-D hot kernel has a smaller radius than cylindrical shape of the 2-D hot kernel. Indeed, the results show that at $t = 138$ μs if gas recirculation is not taken into account (profiles on right side), the ignition kernel propagates through the surrounding fresh mixture.

The temporal evolution of the O, OH and CH_2O mass fractions that remain inside the discharge channel will determine the minimum value of the pulse frequency at which nanosecond discharge pulses should be applied, to successfully ignite and propagate the flame kernel. For example, if plasma discharges are applied at pulse frequencies lower than 5 kHz, (which corresponds to a pulse period higher than 200 μs), both the gas temperature and the concentration of radicals inside the discharge channel become similar to those in the fresh gases. Therefore, the cumulative effect of multiple discharges is minimal. On the other hand, gas recirculation may enhance the initial flame kernel propagation at lower pulse frequencies as it spreads long-lasting intermediate combustion species, such as CH_2O and HCO around the discharge zone. By spreading these intermediate species and increasing the gas energy around the discharge zone, more favorable thermochemical conditions are created. This may explain the flame speed enhancement observed experimentally by Xu et al. [1] when using NRP discharges vs. conventional spark discharges.

4. Conclusions

In the present work we have studied the effect of the gas recirculation generated by a non-equilibrium plasma discharge in a methane-air mixture. 3-D DNS computations, with detailed combustion chemistry and a plasma model developed in our previous work, were performed to better understand the plasma/flow/combustion interactions in mixture ignition by NRP discharges. The results show that the entrainment of fresh gases towards the centre of the discharge channel significantly reduces the hot kernel temperature and increases the diffusion losses due to the evolution of the initially cylindrical kernel into a toroidal shape. The local decrease of the gas temperature and radicals concentration ultimately leads to kernel extinction. This is particularly critical for simulations of ignition by repetitively pulsed discharges at low pulse frequencies. For the present case, the results show that at pulse frequencies lower than 5 kHz, the thermochemical conditions at the centre of the discharge channel, by the time of the following pulse, are similar to those in fresh mixture. Therefore, the synergistic effect of multiple discharges on mixture ignition can only be reached if nanosecond discharges are applied at high pulse frequencies.

Acknowledgment

This research has been supported by Agence Nationale de la Recherche, FAMAC project (Grant no. ANR-12-VPTT-0002) and PLASMAFLAME project (Grant no. ANR-11-BS09-0025). This work was performed using HPC resources from GENCI-IDRIS (Grant no. 2015 - 2b0164). We thank Drs. Da Xu, Philippe Castera and Gabi Stancu for help with the schlieren measurements and Dr. Paul-Quentin Elias for lending us the Schlieren light source.

References

[1] D.A. Xu, D.A. Lacoste, C.O. Laux, *Plasma Chem. Plasm. Process.* (0272–4324) (2015) 1–19.
[2] G. Pilla, D. Galley, D.A. Lacoste, F. Lacas, D. Veynante, C. Laux, *IEEE Trans. Plasm. Sci.,* 34 (6) (2006) 2471–2477.
[3] W. Kim, H. Do, M.G. Mungal, M.A. Cappelli, *Combust. Flame* 153 (4) (2008) 603–615.
[4] I.V. Adamovich, I. Choi, N. Jiang, et al., *Plasma Sour. Sci. Technol.* 18 (3) (2009) 034018.
[5] T. Ombrello, S.H. Won, Y. Ju, S. Williams, *Combust. Flame* 157 (2010) 1906–1915.
[6] W. Sun, M. Uddi, T. Ombrello, S.H. Won, C. Carter, Y. Ju, *Proc. Combust. Inst.* 33 (2011) 3211–3218.
[7] A. Starikovskiy, N. Aleksandrov, *Prog. Energy Combust. Sci.* 39 (1) (2013) 61–110, doi:10.1016/j.pecs.2012.05.003.
[8] S. Barbosa, G. Pilla, D.A. Lacoste, P. Scouflaire, S. Ducruix, C.O. Laux, D. Veynante, *Philos. Trans. Royal Soc. A* (373) (2015) 20140335.
[9] S. Macheret, M. Shneider, R. Miles, in: 36th AIAA Plasmadynamics and Lasers Conference, Toronto, Ontario, Canada, 2005, pp. 2005–5371.
[10] Y. Ju, W. Sun, *Prog. Energy Sci. Combust.* 48 (2015) 21–83.
[11] F. Tholin, D.A. Lacoste, A. Bourdon, *Combust. Flame* 161 (2014) 1235–1246.
[12] M.S. Bak, H. Do, M.G. Mungal, M.A. Cappelli, *Combust. Flame* 159 (10) (2012) 3128–3137.
[13] M. Thiele, J. Warnatz, U. Maas, *Combust. Theory Model.* 4 (4) (2000) 413–434.
[14] M. Thiele, S. Selle, U. Riedel, J. Warnatz, U. Maas, *Proc. Combust. Inst.* 28 (2000) 1177–1185.
[15] M. Castela, B. Fiorina, A. Coussement, O. Gicquel, N. Darabiha, C.O. Laux, *Combust. Flame* 166 (2016) 133–147.
[16] P. Lindstedt, *Proc. Combust. Inst.* 1 (27) (1998) 269–285.
[17] N. Popov, *Plasma Phys. Rep.* 27 (10) (2001) 886–896.
[18] A. Flitti, S. Pancheshnyi, *Eur. Phys. J.* 45 (2009) 21001.

[19] G.D. Stancu, F. Kaddouri, D.A. Lacoste, C.O. Laux, *J. Phys. D: Appl. Phys.* 43 (2010) 124002.
[20] N.A. Popov, *Plasma Phys. Rep.* 37 (9) (2011) 807–815.
[21] I.N. Kosarev, V.I. Khorunzhenko, E.I. Mintoussov, P.N. Sagulenko, N.A. Popov, S.M. Starikovskaia, *Plasma Sources Sci. Technol.* 21 (2012) 045012.
[22] I.V. Adamovich, T. Li, W.R. Lempert, *Philos. Trans. R. Soc. A* 373 (2015) 20140336.
[23] A.M. Starik, B.I. Loukhovitski, A.S. Sharipov, N.S. Titova, *Philos. Trans. R. Soc. A* 373 (2015) 20140341.
[24] J.K. Lefkowitz, P. Guo, A. Rousso, Y. Ju, *Philos. Trans. Ser. A, Math. Phys. Eng. Sci.* 373 (2015) 20140333.
[25] R.C. Millikan, D.R. White, *J. Chem. Phys.* 39 (1963) 3209–3213.
[26] D.L. Rusterholtz, D.A. Lacoste, G.D. Stancu, D.Z. Pai, C.O. Laux, *J. Phys. D: Appl. Phys.* 46 (2013) 464010.
[27] N.A. Popov, in: AIAA Aerospace Sciences Meeting, Grapevine, TX, 7–10 January, 2013, pp. 2013–105251.
[28] A. Coussement, O. Gicquel, J. Caudal, B. Fiorina, G. Degrez, *J. Comput. Phys.* 231 (17) (2012) 5571–5611, doi:10.1016/j.jcp.2012.03.017.
[29] A.W. Cook, W.H. Cabot, *J. Comput. Phys.* 195 (2004) 594–601.
[30] A.W. Cook, W.H. Cabot, *J. Comput. Phys.* 203 (2005) 379–385.
[31] B. Fiorina, S.K. Lele, *J. Comput. Phys.* (222) (2007) 246–264.
[32] D.A. Xu, M.N. Shneider, D.A. Lacoste, C.O. Laux, *J. Phys. D: Appl. Phys.* 47 (23) (2014) 235202.